# Local intracerebral inhibition of IRE1 by MKC8866 sensitizes glioblastoma to irradiation/chemotherapy in vivo

Pierre Jean Le Reste, R Pineau, Konstantinos Voutetakis, J Samal, Gwenaele Jegou, Stéphanie Lhomond, Adrienne M Gorman, Afshin Samali, John B Patterson, Q Zeng, et al.

# Local intracerebral Inhibition of IRE1 by MKC8866 sensitizes glioblastoma to irradiation/chemotherapy *in vivo*.

Pierre Jean Le Reste[1,2,3,4,14], Raphael Pineau[1,2,3,14], Konstantinos Voutetakis[5,6], Juhi Samal[7], Gwénaële Jégou[1,2,3], Stéphanie Lhomond[7,8], Adrienne M. Gorman[7,8], Afshin Samali[8], John B Patterson[9],Qingping Zeng[9], Abhay Pandit[7], Marc Aubry[3,10,11], Nicolas Soriano[3,10], Amandine Etcheverry[11], Aristotelis Chatziioannou[5,12], Jean Mosser[3,10,11,13], Tony Avril[1,2,3], and Eric Chevet[1,2,3,*]

[1]Inserm U1242, University of Rennes, Rennes, France. [2]Centre de lutte contre le cancer Eugène Marquis, Rennes, France. [3]Rennes Brain Cancer Team (REACT), 35000 Rennes, France.[4]Neurosurgery dept, University Hospital of Rennes, 35000 Rennes, France.[5]Institute of Chemical Biology, National Hellenic Research Foundation (N.H.R.F.), Athens, Greece. [6]Department of Biochemistry and Biotechnology, University of Thessaly, Viopolis, 41500, Larissa, Greece; [7]CÚRAM, Centre for Research in Medical Devices, National University of Ireland, Galway, Ireland.[8]Apoptosis Research Centre, National University Ireland Galway, Galway, Ireland.[9]Fosun OrinovePharmaTech Inc., 3537 Old Conejo Road, Suite 104, Newbury Park, CA, 91320, USA.[10]University of Rennes, CNRS, IGDR [(Institut de génétique et développement de Rennes)]-UMR 6290, F-35000 Rennes, France.[11]CHU Rennes, Service de Génétique Moléculaire et Génomique Médicale, Rennes, France.[12]e-NIOS PC, Kallithea-Athens, Greece.[13]University of Rennes, Plateforme GEH, CNRS, Inserm, BIOSIT - UMS 3480, US_S 018, F-35000 Rennes, France.

[14]equal contribution

[*]Correspondance to EC: InsermU1242, Centre de lutte contre le cancer Eugène Marquis, Avenue de la Bataille Flandres Dunkerque, 35042 Rennes, France. Email :eric.chevet@inserm.fr

**Abstract**

Glioblastoma multiforme (GBM) is the most severe primary brain cancer. Despite an aggressive treatment comprising surgical resection and radio/chemotherapy, patient's survival post diagnosis remains short. A limitation for success in finding novel improved therapeutic options for such dismal disease partly lies in the lack of a relevant animal model that accurately recapitulates patient disease and standard of care. In the present study, we have developed an immunocompetent GBM model that includes tumor surgery and a radio/chemotherapy regimen resembling the Stupp protocol and we have used this model to test the impact of the pharmacological inhibition of the endoplasmic reticulum (ER) stress sensor IRE1, on treatment efficacy.

**Introduction**

Glioblastoma multiforme (GBM) is the most severe primary brain cancer and represents more than 15% of primary brain tumors. Despite an aggressive treatment comprising surgical resection and a combination of irradiation and chemotherapy ("Stupp protocol"), patient's survival post-diagnosis remains short with a median overall survival of 15 months [1]. The lack of efficacy of the current treatments is mostly due to the intratumor heterogeneity at diagnosis with the presence of multiple driver alterations [2], as well as to different tumor cell types that exhibit various sensitivity to anti-cancer agents. Finally, it is due to the diffuse nature of GBM tumors that precludes from performing complete resection. Another limitation for the discovery of new improved therapeutic approaches is the lack of a relevant animal model that extensively recapitulates current GBM patient disease and standard of care.

In the past couple of years, we have demonstrated that the Unfolded Protein Response (UPR) plays an instrumental role in GBM development [3-8]. More precisely, we have shown that IRE1, the most conserved UPR sensor, signals in tumor cells to remodel the tumor microenvironment, to favor tumor growth and most likely to alter the response to treatment. We demonstrated that the IRE1/XBP1s (spliced XBP1) axis exhibits pro-oncogenic properties, whereas Regulated IRE1 Dependent Decay of RNA (RIDD) dampens tumor angiogenesis and tumor cell migration/invasion. This observation was then used to stratify GBM patients, where we showed that survival of patients with tumors exhibiting high XBP1s and low RIDD was significantly reduced compared to that of patients with low XBP1s and high RIDD tumors [8]. These observations point toward the IRE1/XBP1s axis as a potentially relevant therapeutic target which, when inhibited in XBP1s high tumors would i) slow down tumor growth by impairing the pro-tumoral remodeling of the tumor stroma and ii) sensitize tumor cells to the current treatments [9].

To further test the potential impact of the pharmacological targeting of IRE1/XBP1, we propose to use an IRE1 RNase inhibitor, MKC8866 [10], already shown to be effective in other cancer models [11], and in preclinical models of GBM. However, the current preclinical GBM models poorly recapitulate the clinical handling of GBM patients, therefore would not be appropriate to test the therapeutic potential of IRE1 inhibition. In the present study, we developed a novel immunocompetent GBM model that involved tumor surgery and a radio/chemotherapy regimen, resembling the Stupp protocol. Furthermore, we used this

unique model to test the therapeutic relevance of IRE1 inhibition on tumor microenvironment and on treatment efficacy.

**Materials and methods**

*Reagents* - All reagents were purchased from Sigma-Aldrich (*St Quentin Fallavier, France*), unless otherwise stated. For immunohistochemistry staining, primary antibodies against vimentin (rabbit monoclonal, used at 1 in 250 dilution) were obtained from Abcam (*Paris, France*); against CD31 (rabbit polyclonal, used at 1/50 dilution) from Bioss Inc. (*Cliniscience, Nanterre, France*); against IBA-1 (rabbit polyclonal, used at 1/50 dilution) from Wako (*Sobioda, Montbonnot, France*); against activated caspase-3 from Cell Signaling (#9661, used at 1/500 dilution) and against KI67 from Novusbio (NB600-1252, used at 1/500 dilution). For Western blot experiments, primary antibodies against ATF4 and phospho-eIF2alpha (PeIF2a) were purchased from Cell Signaling Technology (*Ozyme, St Quentin-en-Yvelines, France*), anti-Calnexin (CNX) antibodies were a kind gift from JJM Bergeron (McGill University, Montreal, Qc, Canada).

*Cell lines* - The GL261 murine glioblastoma cell line was a kind gift from Dr Clavreul (University of Angers, France). These cells were transfected with the plasmid pGL4-Luc and the luciferase-expressing cells stably selected using G418 (the selected line was polyclonal and renamed GL261-Luc). The cells were cultured in Dulbecco's Modified Eagle Medium *(DMEM, Life Technologies, Thermo Fisher Scientific, Courtaboeuf, France)* with the addition of 10% FBS *(Thermo Fisher Scientific)*, and 100 µg/ml of G418 *(Thermo Fisher Scientific)*. The cells were grown in a humidified incubator at 37°C with 5% $CO_2$. The human U87 and derivates (expressing IRE1 variants) GBM cells were grown in DMEM containing 10% FBS. The human U251 GBM cells (used to test the MKC8866-containg gels in vitro, **Figure S1**) were grown in DMEM containing 10% FBS.

*Genome analyses* - Whole Genome Sequencing of the GL261 cell line was performed by Integragen (https://www.integragen.com/fr/). The coverage was 25X for 75% of the mouse genome with a mean depth of 33X. An in-house post-processing was used to filter out candidate germline mutations more consistent with artifacts (Mapping Quality, Base Quality,

Strand Bias, Variant Quality). Ensembl VEP (Variant Effect Predictor, release 87) program processed variants for further annotation using data available in dbSNP (dbSNP146). We detected copy-number variants and allelic imbalances in GL261 using the Control-FREEC algorithm (FREEC-11.5) with the C57BL_6.bam file downloaded from the SANGER FTP server (ftp://ftp-mouse.sanger.ac.uk/current_bams/) as a non-tumor reference sample.

*Transcriptome analyses* - In order to quantify the transcript-level abundances of implanted GL261-derived tumors for the seven experimental conditions (NR:no resected tumors; R:resected tumors without treatment; MKC:treatment with MKC8866 inhibitor; STUPP protocol; STUPP_MKC: STUPP protocol including MKC8866 inhibitor; PARENTAL:GL261 parental; STUPP_GEL: STUPP protocol including gel implantation lacking MKC8866 inhibitor) RNA sequencing was performed by Integragen (https://www.integragen.com/fr/). FastQC (http://www.bioinformatics.babraham.ac.uk/projects/fastqc/) was used for qualitative evaluation of reads with 95% of bases scoring Q30 and above. Transcript-level quantification data were produced using Salmon (v.1.0.0) program [12], installed in Linux server environment (Ubuntu 16.04.6 LTS) by performing mapping of sequence reads to the reference mouse transcriptome (Release M23 - GRCm38.p6). Transcriptome index and quantitation was determined using Salmon (https://salmon.readthedocs.io/en/latest/salmon.html#using-salmon) and the tximport R/Bioconductor package [13] was used to summarize the estimated transcript abundance. For the conversion of mouse gene symbols (mgi_symbol) to human gene symbols (hgnc_symbol) the getLDS() function of biomaRt R package was used retrieving homologous genes after linking of "mmusculus_gene_ensembl" and "hsapiens_gene_ensembl" datasets.

*Transcriptome comparisons with other lines* - Since mice do not show structural homologs for CXCL8 and MMP1 human genes, Cxcl1 and Mmp1a & Mmp1b were used instead, because of their functional similarity [14-16]. The expression profile of U87-MG human glioblastoma cells (WT-wild type) expressing different IRE1 mutants (A414T, P336L, Q780Stop, S769F) and a dominant negative form of IRE1 (DN), under normal and stress conditions (tn; tunicamycin treated), deposited in GEO (Gene Expression Omnibus) [17] (GSE107859 accession number) was compared to that of GL261 parental cell line after cross-platform harmonization, and evaluation of the IRE1 activity signature [9]. For the cross-

platform normalization process, the Shambhala algorithm [18] was performed in R package HARMONY (https://github.com/oncobox-admin/harmony) for a set of 6546 genes in common between the two platforms (Affymetrix microarrays and RNA sequencing). For the exploration of relationships between the samples cluster dendrograms were built using R package ComplexHeatmap [19] and the statistical significance of hierarchical clustering was assessed with bootstrapping method using the R package pvclust [20]. Sample distance matrices to assess the overall similarity between samples were produced using the R function pheatmap() of R pheatmap package [21] with calculation of Euclidean distance between samples and minimization of the total within-cluster variance by Ward's minimum variance method (ward.D2) [22]. Finally, principal component analysis (PCA) on harmonized gene expression data was conducted as previously described [23].

*Cell culture and treatments* - For survival assays, GL261 cells were cultured in 96-well plates at 5,000 cells/well in the presence of increasing amounts of temozolomide (TMZ) (0 to 1000 µM), MKC8866 (0 to 200 µM) with two treatments of radiation at 5 Gy (at day 1 and day 3). After 5 days (for TMZ) or 6 days (for MKC8866) of culture, 20 µl of the WST1 reagent were added to each well. After 4 hours at 37°C, optical densities (OD) were analyzed using spectrophotometry at 450 nm and 595 nm. Specific OD were given by the difference between the OD observed at 450 nm and the OD at 595 nm. Cell viability was calculated by the ratio of the specific OD observes with cells incubated in the presence of different concentration of TMZ and the specific OD observed with cells cultured in medium alone, this information allowed us to determine IC50 values using Prism software (GraphPad). Each experimental point represents at least a triplicate. For protein and RNA extractions, GL261 cells were seeded at a density of $10^6$ cells per dish (6 cm diameter), with two dishes per time point. Cells were treated as described above for 2, 4, 8 and 24 hours. Each experimental point represents at least a triplicate. For protein extraction, cells were lysed using 100 µl of lysis buffer (30 mM Tris-HCl, pH 7.5, 150 mM NaCl, 1.5% CHAPS and Complete™) per plate. Clarified lysates were complemented with 20 µl of 5 times reducing Laemmli sample buffer prior heat-denaturation and used in Western blot experiments with the indicated antibodies (at 1/1000 dilutions). For RNA preparation, cells were lysed using 1ml of Trizol reagent per plate and RNA was extracted according to the manufacturer's instructions (*Thermo Fisher Scientific*) and PCR analyses performed using previously described protocols [24].

*Tumor cell orthotopic implantation* - Tumor cells (GL261-Luc) were implanted into the brain of immunocompetent C57BL/6rJ, 8 weeks old male mice *(Janvier, Laval, France)*. All animal procedures met the European Community Directive guidelines (Agreement B35-238-40 Biosit Rennes, France/ No DIR 13480) and were approved by the local ethics committee and ensuring the breeding and the daily monitoring of the animals in the best conditions of well-being according to the law and the rule of 3R (Reduce-Refine-Replace). GL261-Luc cells were implanted in the mouse brain by intracerebral injection followed by tumor growth monitoring using bioluminescence. The mice were anesthetized intraperitoneally (i.p.) and then fixed on a stereotactic frame. This framework makes it possible to manipulate the brains of living animals, and to reach isolated areas of the brain precisely relative to markings visible to the naked eye through the use of three-dimensional coordinates. After incising the scalp, the stereotaxic coordinates were calculated for injection of tumor cells into a specific point of the brain, and reproducible for all the mice used. In the study, the tumor cells ($2.5 \times 10^4$ cells per mice in 1 µL) were injected at 2.2 mm to the left of the bregma and 3.2 mm deep to perform the implantation at the level of the striatum.

*Bioluminescence* - Mice were assessed with *in vivo* bioluminescence imaging every 3 days, for the first week, and weekly onward for tumor progression and followed for signs of neurologic deterioration daily. Mice were injected i.p. with 100 µl of luciferin (*Promega, Charbonnières-les-Bains, France*). The luciferin was allowed to circulate for 10 min before the mice were anesthetized with a mix of $O_2$ and isoflurane (2.5%). Mice that showed an increase in tumor burden based on imaging during the first week after tumor implantation were included in the study. Bioluminescence analysis was used to determine the window of resection (day 14).

*Resection* - The mice were anesthetized by the intraperitoneal route with 90 µl of anesthetic (1.5 mg/kg of ketamine and 150 µg/kg of xylazine). Then they were attached to the stereotaxic frame and the scalp was incised to expose the convexity of the skull and the injection point. The opening of the bone was performed with thin forceps allowing minimal craniectomy. Visualization of the tumor was enhanced by using an injection of intravenous fluorescein at the beginning of the procedure. Thanks to a UV source, this fluorophore

makes possible to visualize the zones of rupture of blood-brain barrier characteristic of glioblastoma. This visual aid makes it possible to delineate the tumor borders and thus minimizes the lesions on healthy parenchyma. The resection was performed using a surgical microscope, and the tumor was aspirated with the help of a small suction. The extent of resection was mainly driven by the depth of the tumor. Once the resection was performed, the hole left by the tumor was filled with a fibrin-collagen gel containing the inhibitor of interest. The craniectomy was closed with the help of a teflon patch (Neuropatch®) slid under the skull, fixed by the application of biocompatible acrylic glue. This step allows maintenance of intracranial pressure and prevents tumors from developing in the subcutaneous space. Finally, the skin was sewn with non-resorbable monofilament sutures at the end of the procedure (see **Movie S1**).

*Stupp-like treatment applied to mice* – Three days after the resection, we proceeded to apply the Stupp-like protocol, consisting in two steps including (i) concomitant radio/chemotherapy: mice were anesthetized with Isoflurane, and placed in a lead dome to cover the entire animal to prevent ionizing radiation from reaching the healthy tissues of the animals. A hole of a few centimeters was made in the lead dome, corresponding to the resection area of the tumor, in order to irradiate only the area of interest. The animals were subjected to a radiation of 5 times 2Gy 3 days after resection along with 25 mg/kg/day of TMZ delivered intraperitoneally followed by (ii) stand-alone chemotherapy. In the latter procedure animals were subjected to the standard procedure of chemotherapy, namely 30-50 mg/kg of TMZ on 5 days with 2 or 3 days of rest between each treatment. Survival was measured as the time between implantation and sacrifice, which was performed by cervical dislocation in case of critical clinical signs or loss of weight >15%.

*Immunohistochemistry* - The immunochemistry experiments were performed on 5 µm tumor sections which were incubated at room temperature for 1 hour with primary antibodies. Immunostaining was performed using BenchMarkXT-Ventana Medical Systems with kit OMNIMAP (system " biotin-free" using multimer technology) with antigen retrieval for all (Tris/borate/EDTA pH 8). To perform the analysis, glass slides were converted on to digital slides with the scanner Nanozoomer 2.0-RS Hamamatsu. The quantification of the necrosis was carried out from HES using the NIS-Elements software (Nikon). Immunohistochemistry

was performed with anti IBA1 (macrophages and microglial cells), anti CD31 (endothelial cells) antibodies as previously described [9]. Cell death and proliferation were determined using anti activated caspase-3 and anti KI67 antibodies, respectively.

*Manufacturing of the gel implant containing the IRE1 RNase inhibitor MKC8866 and cell-based testing* - Human fibrinogen was dissolved in deionized water at a concentration of 30 mg/ml followed by dialysis against tris-buffered saline (TBS) overnight. MKC8866 was resuspended in the fibrinogen component of fibrin microgels at a final concentration of 10 and 100 µM. The gel-forming fraction containing MKC8866 was then dispensed as 7 µl droplets on a hydrophobic surface (commercial Teflon® tape) to create a micro-droplet. The gel fractions were then crosslinked by human thrombin (40 U/ml) and incubated for 20 minutes at 37 °C for stable cross-linking. To test the gel in vitro, U251 cells were seeded in 12-well plates at 10,000 cells/well or 20,000 cells/well. After 24h, the cells were cultivated in the absence (no gel) or presence of fibrin microgel containing different concentrations of MKC8866 (0 to 100 µM). After seven days, the cells were treated for 5h with tunicamycin at 5 µg/mL to activate IRE1 pathway and XBP1 RNA splicing. They were then lysed using 0.5 ml of Trizol reagent per well and RNA was extracted according to the manufacturer's instructions (Thermo Fisher Scientific). PCR was performed for total XBP1 splicing, and the resulting amplified DNA products were resolved using a 4% agarose gel. The upper band (unspliced XBP1) and lower band (spliced XBP1) were then quantified using the ImageJ software and the ratio between the unspliced (U) and spliced (S) forms of XBP1 were calculated by the following formula: S/(U+S) *100. For in vivo studies, gel implantation was carried out at the moment of the surgery. Briefly preformed microgels were deposited in the resection cavity prior to implanting a teflon plate and sewing the skin.

*Statistical analyses* - All the statistical analyses were performed using the GraphPad Prism software and the Mann-Whitney test.

**Results**

*Qualification of GL261 murine GBM as a relevant model for in vivo studies with IRE1 inhibitors*

Since we previously showed that activation of IRE1 signaling (and in particular of the IRE1/XBP1 arm) was linked to GBM aggressiveness by promoting tumor-supporting immune cells, angiogenesis and migration/invasion of the tumor cells [8], we reasoned that a relevant *in vivo* mouse model should i) use GBM cells exhibiting high IRE1 activity, ii) be immunocompetent and iii) be subjected to a treatment similar to the standard of care in human. As such our first objective was to identify a mouse GBM cell line that could be considered as relevant. To this end we investigated the activation status of the IRE1 pathway in the mouse GL261 line. We compared the mouse line to the human U87 line expressing various mutants of IRE1 and treated or not with the ER stressor tunicamycin (**Figure 1A**) [8]. A principal component analysis revealed that GL261 co-clustered with U87, overexpressing the wild type IRE1 or the P336L mutant (in which IRE1 is constitutively activated), treated or not with tunicamycin, thereby indicating that the IRE1 pathway might be constitutively activated in GL261 cells as previously observed in other cell lines [8]. This result was confirmed by the use of the IRE1 activity signature [8]. Using hierarchical clustering, we confirmed that GL261 cells exhibited an IRE1 activation profile similar to XBP1+/RIDD+ when comparing to the profiles previously established with human primary GBM lines [8] (**Figure 1B, C**). To further document the genetic characteristics of the GL261 line, we focused on 86 GBM related genes (including variants, **Tables S1-S3**), including 79 genes recently reported [25], and 7 additional genes (two Stupp protocol response predictors *Mgmt* and *Dgki*; the canonical Endoplasmic Reticulum stress sensors *Eif2ak3* (*Perk*), *Atf6* and *Ern1* (*Ire1*); the genes *Pi3k* and *Tert* frequently mutated in IDH-wild type GBM). We found that 17 of these genes were harboring one or more mutations with a predicted functional impact (**Table 1**). Some of those mutated genes are known oncogenes (*Kras*, *Met*, *Pi3kca*) or tumor suppressor genes (*Nf1* and *Trp53*). Cancer genes were also affected by DNA gains (*Egfr*, *Mdm2*, *Pdgfra* for instance) or losses (*Cdkn2c* and *Pten*). RNAseq of the parental GL261 cells further indicated that oncogenic mutations were present and sometimes enriched at the mRNA level in those cells (*Kras*, *Nf1*, *Pik3ca* and *Trp53* for instance, **Table 1, Figure 1D, Tables S1-S3**). Interestingly, the Kras mutation is found in 2% of the human GBM tumors and the pathway is activated in more than 50% of the tumors [8]. These results indicated that GL261 cells express known GBM cancer driver genes, can be used in syngeneic models (in C57BL/6 mice), exhibit a high basal IRE1 signaling and therefore represent a suitable cell line for the development of an *in vivo* model relevant to test the impact of IRE1 inhibition as an adjuvant

therapeutic strategy. Of note, GL261 exhibited some features of the mesenchymal sub-type of GBM when their properties (at both genome and transcriptome levels) were analyzed and compared to U87 cells or other primary GBM lines [8].

*Novel preclinical GBM mouse model including surgery, irradiation and chemotherapy*

Due to lack of a murine preclinical model recapitulating GBM patients' handling, we sought to develop a novel model that would comprise surgical resection combined with radio/chemotherapy, comparable to the clinical setup (**Figure 2A,** human vs. mouse). We designed an experimental approach relying on the mouse GBM line GL261 that we modified for stable expression of luciferase, in order to allow live tumor imaging. These cells were then orthotopically injected in C57BL/6 mouse brain and tumors allowed to grow for 12 to 13 days. At this stage, tumors were surgically resected using fluorescein as a tumor tracer (**Movie S1**) and the mice were allowed to recover from surgery for 1 week before undergoing Stupp-like treatment (**Figure 2B**). The Stupp-like protocol included radiation (2 Gy/day, 5 exposures) combined with chemotherapy (TMZ, 25 mg/kg, 5 applications) and followed by TMZ treatment alone (30-50 mg/g, 5 applications followed by 2 days without treatment for 4 weeks). Following the completion of Stupp-like procedure, described in **Figure 2**, mice were sacrificed at first clinical signs. Brains were collected, fixed in paraformaldehyde (PFA 4%), embedded in paraffin prior to immunohistochemical analysis using anti-vimentin antibodies. This revealed the impact of surgery on tumor size and aggressiveness (**Figure 3A**), as well as the effects of irradiation/TMZ treatment, which appeared to reduce tumor size and ability to infiltrate surrounding parenchyma (**Figure 3A**, SIT). Mouse survival was then evaluated upon these treatments (**Figure 3B**), and showed that while surgery did not have any significant impact, Stupp-like treatment doubled mouse survival, thereby recapitulating observations made in patients following this protocol. Moreover, we analyzed the impact of surgery on tumor angiogenesis by staining the recurring tumor sections with anti-CD31 antibodies (**Figure 3C, arrows**). Quantitation of the staining revealed that there was no significant difference in blood vessel density between the non-resected and resected conditions (**Figure 3D**), however more work should be carried out to provide an in depth analysis of the nature of the blood vessels analyzed in both conditions even though tumor angiogenesis appeared abnormal. Furthermore, we analyzed the ability of tumor cells to invade the neighboring parenchyma in primary or post-surgery

recurring tumors, by analyzing the vimentin staining (**Figure 3E, arrows**). Quantitation of this staining revealed that surgical resection of tumors enhanced the capacity of tumor cells to infiltrate non-tumor tissue (**Figure 3F**).

*Impact of IRE1 RNase inhibitor MKC8866 in vitro and in vivo*

Once this model was established, we next sought to evaluate the impact of pharmacological IRE1 inhibition on the parameters mentioned above. Since GL261 appear to express MGMT [26] in an IRE1-independent manner, this might explain the high concentration of TMZ needed to kill them (IC50 ~ 800 μM). First, to document the effects of MKC8866 on GL261 cells *in vitro*, we evaluated whether MKC8866 blocked ER stress induced by tunicamycin (TUN, an inhibitor of protein N-glycosylation and inducer of ER stress). As expected MKC8866 treatment impaired IRE1 signals as assessed by the inhibition of XBP1 mRNA splicing upon treatment with the N-glycosylation inhibitor tunicamycin (TUN; **Figure 4A**, top). We next evaluated how TMZ affected XBP1 mRNA splicing using the same approach and did not detect any impact of the drug (TMZ; **Figure 4A**, bottom). These results were also observed at the level of XBP1s protein, whose expression was undetectable upon TMZ treatment (8h) but increased upon TUN (8h; and dampened upon MKC8866 treatment). To further document these results, we evaluated the expression of a genuine XBP1s target gene, ERdj4. ERdj4 expression increased dramatically upon TUN treatment with kinetics compatible with the activation of XBP1s and attenuated upon MKC8866 treatment (**Figure 4B**). No major change was observed upon TMZ treatment. MKC8866 did not affect TUN-induced ATF4 expression (**Figure 4C**, top panel) indicating that MKC8866 did not impact on PERK signaling, another ER stress sensor. We next evaluated the stress induced upon TMZ treatment (performed at the EC50) and how MKC8866 impacted TMZ-induced UPR signaling (**Figure 4C-D**). This showed that TMZ treatment impacted on ATF4 expression and that this was altered in the presence of MKC8866 (**Figure 4C**, bottom panel), likely reflecting the impact of DNA damaging agents on RIDD activity as previously reported [27]. Notably, activation of three UPR branches IRE1, PERK and ATF6 also appeared to be altered in response to TMZ, since the expression of UPR-target gene was modified (**Figure 4D**). Finally, since treatment of GL261 cells with MKC8866 appeared to impact on the response of these cells to different stressors, we evaluated the impact IRE1 RNase inhibition on cell sensitivity to TMZ. To do so, TMZ IC50 was determined for GL261 and evaluated to be of about 800 μM

(**Figure 4E**), and did not vary upon combined radiation. GL261 cells' sensitivity to TMZ was increased upon treatment with MKC8866, phenomenon further amplified with combined irradiation (**Figure 4E**). These results suggest that TMZ-induced damages to the cells promote the activation of IRE1 dependent adaptive signals that if blocked by MKC8866, decrease the cell ability to cope with TMZ treatment. Consequently, these data suggest that combining Stupp-like treatment with MKC8866 might be an interesting approach to enhance treatment efficacy.

A major hurdle in using MKC8866 for *in vivo* applications in the brain lies in the fact that this IRE1 inhibitor, previously demonstrated to impact tumor growth in other cancer models [11], does not pass the blood brain barrier (BBB) and as such would not be suitable for intervention in brain tumors. To overcome this problem, we reasoned that we could take advantage of the surgical resection step for selective intra-operative delivery of IRE1-targeting drugs, provided that proper biomaterial scaffolds would be used to allow controlled release of the drugs to the tumor. The procedure was successfully set in place using a drug containing fibrin microgel. The plugs of 2 $mm^3$ were appropriate in terms of size and conformation, they adjusted perfectly to the resection cavity. This drug-containing device alone neither impacted on tumor development (without Stupp-like treatment) nor on mouse survival following resection when containing MKC8866 (not shown). To test whether the adjuvant use of MKC8866 could impact on mouse survival, we evaluated the combination of this inhibitor with Stupp-like treatment using the fibrin-collagen gel plug as delivery tool. Surgery and drug implant were carried out and the first line of treatment including radiation/chemotherapy was done in the previous series of experiments (**Figure 5A**). Mouse survival was evaluated and brains were collected as sacrifice. In the first instance we evaluated the impact of MKC8866, Stupp-like treatment and combined therapy on tumor morphology at sacrifice. Tumors developing in the presence of the MKC8866 containing plug and upon Stupp-like treatment presented a totally different phenotype from those developing under Stupp-like treatment alone. This phenotype corresponded to much smaller tumors with tumor escape significantly delayed (**Figure 5B**). Furthermore, when necrosis was measured in tumors collected at sacrifice (H&E staining, **Figure 5C**, bottom), we observed that the combination of Stupp-like treatment and MKC8866 yielded much important necrosis, reflecting treatment efficacy (**Figure 5C**). At last, we tested whether combined MKC8866 and Stupp-like treatment impacted on mouse survival. This allowed us to establish

survival curves (**Figure 5D**) that demonstrate the positive impact of MKC8866 contained fibrin/collagen graft (1-2 μl) either at a 10 μM (**Figure 5D**, green) or 100 μM (**Figure 5D**, orange) concentration on the efficiency of Stupp-like treatment. We found that MKC8866 yielded a significant increase of mice survival (of about 20%) compared to Stupp alone, however with no significant impact of the drug concentration used in the gel (**Figure 5D)** whereas it was observable in cell culture (**Figure S1**). This suggested that the main limitation in our experimental design was the capacity of the fibrin/collagen gel to control the delivery of the drug over time. Collectively, our results show that IRE1 RNase inhibition might represent an appealing approach to enhance the efficiency of current treatments towards GBM and that further work is needed to improve drug delivery to the tumor site. We next analyzed how tumors responded to the different treatments using immunohistochemical analyses of apoptosis (activated caspase 3, **Figure 6A**), proliferation (KI67, **Figure 6B**), tumor infiltration by macrophages and microglial cells (IBA1, **Figure 6C**), tumor vascularization (CD31, **Figure 6D**). An representative image of the staining observed in each condition is provided (**Figure 6A-D**, left panels). All tumor sections analyzed (9 fields on 3 independent tumor sections) were quantified as described in the Methods section and quantitation is provided (**Figure 6A-D**, right panels). Our results show that in our experimental conditions, the only significant effect with MKC8866 was an increased apoptosis in response to Stupp treatment. This is consistent with the observed increased tissue necrosis shown in **Figure 5**. In addition, tumor infiltration by macrophage or microglial cells was significantly reduced in tumors exposed to Stupp treatment in the presence of MKC8866 (**Figure 6C**). These results are consistent with our previous results suggesting the pro-inflammatory role of IRE1 signaling in tumor cells [9], however, whether macrophage infiltrate is tumor promoting or tumor suppressive remains to be clearly established.

At last, three tumors from each group collected at sacrifice were dissociated and dissociated cells grown in culture to isolate GL261-derived lines following various treatments. These lines were then evaluated for their ability to proliferate (**Figure 7A**, bottom panel). This showed that except for cells derived from non-resected tumors which proliferated faster, none of the other lines showed any variation compared to the parental line, this result was similar to that observed with the sensitivity of cells to MKC8866 (**Figure 7A**, top panel). In contrast, all GL261-derived lines exhibited a higher sensitivity to TMZ than the parental line with the most striking observation with the lines derived from tumors

relapsing after resection (**Figure 7A**, middle panel). It is interesting to note that lines derived from tumors treated with Stupp-like and MKC8866 showed great heterogeneity of response, a result contrasting with other lines. The tumor cell selection process post-resection in those conditions (STUPP and STUPP+MKC) at sacrifice might induce a strong bias in the nature of the cells collected. To investigate if this heterogeneity was reflected at the level of the transcriptome, lines were analyzed using RNAseq and then clustered based on IRE1 activity signature (**Figure 7B**). This revealed that treatment of the animals does not seem to impact on the basal IRE1 activity in tumor-derived GL261 cells grown in culture. This result might suggest that the alterations resulting from the treatment do not directly impact on basal IRE1 activity thereby suggesting that global functional analysis of these cells' transcriptomes would be relevant to analyze further to identify the affected pathways.

**Discussion**

Herein, we established a novel murine preclinical model of GBM that recapitulates standard therapy of human patients. This model includes surgical resection of the tumor and Stupp-like treatment combining irradiation and TMZ-based chemotherapy. Our model relies on the use of GL261 cells that exhibit a genome harboring the majority, if not all mutations, driving gliomagenesis. These mutations and/or copy number variations were observed in genes involved in the 3 main pathways affected in GBM (the receptor tyrosine kinase (RTK), P53, RB1 pathways, **Figure 1** [28]). Furthermore, GBM related genes harboring one SNV in GL261 and two DNA copies (**Tables S1-S3**) had variable mutation allele frequency (MAF) values ranking between 6 and 100%. This MAF distribution strongly suggests that multiple, different clones compose the parental GL261 line (up to 5). Altogether these GL261 characteristics recapitulate molecular features observed for primary GBM at diagnostic with the presence of multiple drivers and/or multiple GBM clones [2]. Importantly, we shown that GL261 displayed a constitutive activation of IRE1, likely resembling some primary GBM lines previously described [2]. Therefore, this cell line very likely constitutes a valuable GBM model for preclinical studies in mice, and in particular to study IRE1 inhibitors.

One of the main advantage of our model is the implantation of a very standardized surgical procedure very close to human surgery. This step brought some constraints in the choice of the mouse model. We chose a syngeneic model allowing an immune response

rather than the widely used U87 xenograft. Furthermore, U87 cell lines produce well-defined tumors with low invasive properties, making them non relevant for a pertinent surgical model, where GL261 form tumors with a macroscopic and invasive behavior very close to human glioblastoma. PDX models appear as an interesting option allowing a more realistic modeling of human glioblastomas than the strictly murine GL261 model. However, the tuning of these models is usually longer and more complex than for the syngeneic ones, and the growth of the tumors appear significantly slower. Furthermore, the GL261 cell line is widely available, making the reproducibility of this model easier. Now that our model is well calibrated, the next steps of development will include PDX models to take into account the great heterogeneity of human glioblastoma. One last alternative to our mice model would have been the use of genetically engineered models for a more physiological tumor environment, but these models do not provide standardized tumor localization which is a major feature for surgical accessibility and prognosis.

The use of such a model in the context of our discovery regarding the role of IRE1 signaling in GBM, has allowed us to test the impact of IRE1 pharmacological inhibition in enhancing the efficacy of Stupp-like treatment as already demonstrated in other contexts, for instance for the sensitization of Triple Negative Breast Cancers (TNBC) to paclitaxel therapy [11, 29]. In contrast with the approaches carried out with TNBC which included systemic injection of MKC8866 [11, 29], the available pharmacological inhibitors did not pass the blood brain barrier and as such we had to design a novel type of therapeutic strategy which would allow the controlled release of the drug during Stupp-like treatments. As such, we took advantage of the surgical step to use the peri-surgical implantation of a biocompatible graft containing the drug. This was achieved by using a fibrin/collagen graft (1-2 μl) containing 10 μM (**Figure 5D**, green) or 100 μM (**Figure 5D**, orange) of MKC8866, corresponding to non-toxic concentrations in cell culture and in animals. The grafts were implanted at the time of surgery and mice were then exposed to Stupp-like treatments. Both macroscopic exploration, immunohistochemistry and Kaplan-Meier survival curves (**Figure 5**) indicated that combination of MKC8866 with Stupp-like treatment enhanced its efficacy, leading to increased necrosis within the tumor and to prolonged mouse survival. At last, the observed effects of TMZ on the activation of the UPR arms (ATF4, XBP1s and UPR target genes) might reflect the impact of DNA damaging agents on UPR activation [11, 29], and will

require an in-depth investigation to be fully characterized. The impact of MKC8866 on TMZ-induced UPR signals also suggests important cross-talks between the different arms.

Collectively, our work provides the proof of concept that the pharmacological inhibition of IRE1 could be used as an adjuvant to enhance the efficacy of combined radiation and chemotherapy in the context of GBM. However, one still must evaluate the impact of these treatments on the characteristics of the recurrent tumors regarding their treatment resistance properties. Also, of note is to investigate whether specific strata from cohorts of GBM patients (e.g., depending on their IRE1 signaling characteristics) would derive more benefit and should be preferentially targeted.

**Acknowledgements**

We thank the BIOSIT H2P2 platform and Florence Jouan for immunohistochemistry and the BIOSIT Animal facility ARCHE (https://biosit.univ-rennes1.fr/). This work was funded by grants from the French National Cancer Institute (INCa, PLBIO2017, 2019, 2020), the Fondation pour la recherche Médicale (FRM ; équipe labellisée 2018) to EC and EU H2020 MSCA ITN-675448 (TRAINERS) and MSCA RISE-734749 (INSPIRED) grants to AS, AC and EC. The work was also supported in part by research grant from Science Foundation Ireland (SFI), co-funded under the European Regional Development Fund under Grant number 13/RC/2073.

**Authors' contributions**

**Conceptualization** – PJLR, RP, EC; **Data curation** – MA, NS, KV, AE, JM; **Formal analysis** – MA, NS; **Funding acquisition** – EC, AP, AS, AG; **Investigation** – PJLR, KV, RP, GJ, SL, MA, NS, AE, JM, TA; **Methodology** – PJLR, RP,KV, EC; **Project administration** – PJLR, RP, TA, EC; **Resources** – JS, AP, JBP, AC, QZ; **Supervision** – EC; **Validation** – PJLR, RP, EC; **Visualization** – PJLR, RP, KV, GJ, SL, MA, NS, AE, AC, JM, EC; **Writing – original draft** – EC; **Writing – review & editing** – PJLR, RP, SL, AG, AS, MA, NS, AE, JM, AC, TA, EC (established according to https://casrai.org/credit/)

**Conflicts of interest**

EC, AS, AG are founding members of Cell Stress Discoveries ltd (https://cellstressdiscoveries.com/). AC is founding member of e-NIOS Applications PC (https://e-nios.com/).

**References**


1. Stupp, R., et al., *Radiotherapy plus concomitant and adjuvant temozolomide for glioblastoma.* The New England journal of medicine, 2005. **352**: p. 987-96.
2. Körber, V., et al., *Evolutionary Trajectories of IDHWT Glioblastomas Reveal a Common Path of Early Tumorigenesis Instigated Years ahead of Initial Diagnosis.* Cancer Cell. . 2019. **35**(4): p. 692-704.
3. Drogat, B., et al., *IRE1 signaling is essential for ischemia-induced vascular endothelial growth factor-A expression and contributes to angiogenesis and tumor growth in vivo.* Cancer Res, 2007. **67**(14): p. 6700-7.
4. Auf, G., et al., *Inositol-requiring enzyme 1alpha is a key regulator of angiogenesis and invasion in malignant glioma.* Proc Natl Acad Sci U S A, 2010. **107**(35): p. 15553-8.
5. Dejeans, N., et al., *Autocrine control of glioma cells adhesion and migration through IRE1alpha-mediated cleavage of SPARC mRNA.* J Cell Sci, 2012. **125**(Pt 18): p. 4278-87.
6. Pluquet, O., et al., *Posttranscriptional regulation of PER1 underlies the oncogenic function of IREalpha.* Cancer Res, 2013. **73**(15): p. 4732-43.
7. Obacz, J., et al., *Endoplasmic reticulum proteostasis in glioblastoma-From molecular mechanisms to therapeutic perspectives.* Sci Signal, 2017. **10**(470).
8. Jabouille, A., et al., *Glioblastoma invasion and cooption depend on IRE1α endoribonuclease activity.* Oncotarget, 2015. **22**(28): p. 24922-34.
9. Lhomond, S., et al., *Dual IRE1 RNase functions dictate glioblastoma development.* EMBO Mol Med, 2018. **10**(3).
10. Volkmann, K., et al., *Potent and selective inhibitors of the inositol-requiring enzyme 1 endoribonuclease.* J Biol Chem, 2011. **286**(14): p. 12743-55.
11. Logue, S.E., et al., *Inhibition of IRE1 RNase activity modulates the tumor cell secretome and enhances response to chemotherapy.* Nat Commun, 2018. **9**(1): p. 3267.
12. Patro, R., et al., *Salmon provides fast and bias-aware quantification of transcript expression.* Nat Methods, 2017. **14**(4): p. 417-419.
13. Soneson, C., M.I. Love, and M.D. Robinson, *Differential analyses for RNA-seq: transcript-level estimates improve gene-level inferences.* F1000Res, 2015. **4**: p. 1521.
14. Foley, C.J., et al., *Matrix metalloprotease-1a promotes tumorigenesis and metastasis.* J Biol Chem, 2012. **287**(29): p. 24330-8.
15. Girbl, T., et al., *Distinct Compartmentalization of the Chemokines CXCL1 and CXCL2 and the Atypical Receptor ACKR1 Determine Discrete Stages of Neutrophil Diapedesis.* Immunity, 2018. **49**(6): p. 1062-1076 e6.
16. Shea-Donohue, T., et al., *Mice deficient in the CXCR2 ligand, CXCL1 (KC/GRO-alpha), exhibit increased susceptibility to dextran sodium sulfate (DSS)-induced colitis.* Innate Immun, 2008. **14**(2): p. 117-24.
17. Edgar, R., M. Domrachev, and A.E. Lash, *Gene Expression Omnibus: NCBI gene expression and hybridization array data repository.* Nucleic Acids Res, 2002. **30**(1): p. 207-10.
18. Borisov, N., et al., *Shambhala: a platform-agnostic data harmonizer for gene expression data.* BMC Bioinformatics, 2019. **20**(1): p. 66.
19. Gu, Z., R. Eils, and M. Schlesner, *Complex heatmaps reveal patterns and correlations in multidimensional genomic data.* Bioinformatics, 2016. **32**(18): p. 2847-9.

20. Suzuki, R. and H. Shimodaira, *Pvclust: an R package for assessing the uncertainty in hierarchical clustering.* Bioinformatics, 2006. **22**(12): p. 1540-2.
21. Kolde, R., *R package version 1.0.12-pheatmap: Pretty Heatmaps*. 2019.
22. Szekely, G.J. and M.L. Rizzo, *Hierarchical Clustering via Joint Between-Within Distances: Extending Ward's Minimum Variance Method.* Journal of Classification, 2005. **22**(2): p. 151-183.
23. Wickham, H., *ggplot2: Elegant Graphics for Data Analysis*. 2016, Springer-Verlag New York.
24. Sicari, D., et al., *A guide to assessing endoplasmic reticulum homeostasis and stress in mammalian systems.* FEBS J, 2019. **doi: 10.1111/febs.15107**.
25. Lee, J.H., et al., *Human glioblastoma arises from subventricular zone cells with low-level driver mutations.* Nature, 2018. **560**(7717): p. 243-247.
26. Tao, S., et al., *TGF-β/Smads Signaling Affects Radiation Response and Prolongs Survival by Regulating DNA Repair Genes in Malignant Glioma.* DNA Cell Biol, 2018. **11**(37): p. 909-916.
27. Dufey, E., et al., *Genotoxic stress triggers the activation of IRE1α-dependent RNA decay to modulate the DNA damage response.* Nat Commun, 2020. **11**(14): p. 2401.
28. Brennan, C.W., et al., *The somatic genomic landscape of glioblastoma.* Cell, 2013. **155**(2): p. 462-77.
29. Zhao, N., et al., *Pharmacological targeting of MYC-regulated IRE1/XBP1 pathway suppresses MYC-driven breast cancer.* J Clin Invest, 2018. **128**(4): p. 1283-1299.

**Table 1: GBM related genes harboring one or more mutations with a predicted functional impact using Ensembl Variant Effect Predictor.**

| Gene | Chr | POS | Exon | Wild/Mut | Csq | IMPACT | SIFT | Grantham | WGS depth | WGS MAF | Protein V | RNAseqDepth | RNAseq MAF | Pathway |
|---|---|---|---|---|---|---|---|---|---|---|---|---|---|---|
| Arid1a | 4 | 133681286 | 20 | tGt/tAt | missense V | MODERATE | . | 194:R | 20 | 30 | C1966Y | 130 | 45 % | SWI/SNF chromatin remodeling |
| Arid1b | 17 | 4995695 | 1 | Ggc/Tgc | missense V | MODERATE | . | 159:R | 23 | 30 | G201C | 4 | 0 % | SWI/SNF chromatin remodeling |
| Card6 | 15 | 5099251 | 4 | Gca/Cca | missense V | MODERATE | deleterious | 27:C | 68 | 16 | A888P | 41 | 7 % | apoptosis/NF-kB |
| Gabra6 | 11 | 42320453 | 2 | Gaa/Taa | stop | HIGH | . | 250 | 33 | 27 | E30 | 0 | 0 % | -- |
| Gpx5 | 13 | 21287385 | 5 | aGc/aCc | missense V | MODERATE | deleterious | 58:MC | 30 | 47 | S216T | 0 | 0 % | -- |
| Il18rap | 1 | 40524376 | 4 | Cat/Aat | missense V | MODERATE | tolerated | 68:MC | 10 | 7 | H22N | 0 | 0 % | immune response/NF-kB |
| Kras | 6 | 145246772 | 2 | Ggt/Tgt | missense V | MODERATE | deleterious | 159:R | 36 | 100 | G12C | 142 | 100 % | RTK/MAPK |
| Met | 6 | 17491881 | 3 | tCg/tTg | missense V | MODERATE | deleterious | 145:MR | 8 | 6 | S214L | 48 | 2 % | RTK |
| Mgmt | 7 | 137127888 | 5 | Ccc/Acc | missense V | MODERATE | deleterious | 38:C | 20 | 15 | P144T | 0 | 0 % | DNA repair |
| Mmp13 | 9 | 7272774 | 2 | Aaa/Caa | missense V | MODERATE | tolerated | 53:MC | 40 | 70 | K45Q | 0 | 0 % | infiltration/ECM degradation |
| Nf1 | 11 | 79471575 | 34 | aGt/aTt | missense V | MODERATE | deleterious | 142:R | 45 | 29 | S1526I | 27 | 70 % | RTK/MAPK |
| Nf1 | 11 | 79546350 | 41 | Gag/Tag | stop | HIGH | . | 250 | 12 | 8 | E2031 | 34 | 44 % | RTK/MAPK |
| Nlrp5 | 7 | 23418216 | 7 | tcG/tc | frameshift V | HIGH | . | . | 31 | 58 | S455X | 0 | 0 % | -- |
| Pik3ca | 3 | 32439942 | 4 | aTt/aCt | missense V | MODERATE | tolerated | 89:MC | 39 | 46 | I351T | 55 | 31 % | RTK/AKT |
| Rfx6 | 10 | 51693701 | 5 | cAt/cGt | missense V | MODERATE | deleterious | 29:C | 41 | 100 | H190R | 0 | 0 % | -- |
| Rfx6 | 10 | 51715912 | 11 | Ttt/Att | missense V | MODERATE | deleterious | 21:C | 28 | 50 | F348I | 0 | 0 % | -- |
| Scn9a | 2 | 66487583 | 26 | atG/atT | missense V | MODERATE | tolerated | 10:C | 27 | 26 | M1509I | 0 | 0 % | Na+ channel |
| Scn9a | 2 | 66566238 | 3 | Cct/Act | missense V | MODERATE | tolerated | 38:C | 30 | 73 | P104T | 0 | 0 % | Na+ channel |
| Sema3e | 5 | 14236370 | 14 | cCg/cAg | missense V | MODERATE | deleterious | 76:MC | 18 | 67 | P535Q | 27 | 93 % | angiogenesis |
| Trp53 | 11 | 69588455 | 5 | cGt/cCt | missense V | MODERATE | tolerated | 103:MR | 23 | 100 | R153P | 367 | 100 % | p53 |

Csq: predicted effect that the allele of the variant may have on the transcript. IMPACT: a subjective classification of the severity of the variant consequence, based on agreement with SNPEff (HIGH/MODERATE/LOW).

**Figures legends**

**Figure 1: Selection of GL261 as a relevant model for testing the relevance of IRE1 inhibition in GBM. A**) Biplot projection of PC3 and PC4 components of PCA analysis on harmonized gene expression data of GL261 parental and U87 IRE1_WT, IRE1_DN and IRE1 mutant clones under normal and stress conditions. **B**) Hierarchical clustering heatmap of GL261 parental and U87 IRE1_WT, IRE1_DN and IRE1 mutant cell lines with tunicamycin (tn) and without stress based on the harmonized gene expression profile of IRE1 signature. Pearson correlation coefficient was used for sample distance correlation and the average agglomeration method was used for sample clustering. U87 cells in normal and stress conditions are represented with pink and yellow bars to the top of the heatmap while the GL261 parental cell line is represented with the grey box. **C**) Sample distance matrix of GL261 parental and U87 IRE1_WT, IRE1_DN and IRE1 mutant cell lines under normal and stress conditions, based on the harmonized gene expression profile of IRE1 signature using the Euclidean distance between samples. For sample hierarchical clustering Ward's minimum variance method (ward.D2) was used. **D**) Sequence mutations and copy number changes are depicted as grey boxes for mutations, red boxes for gain of DNA copy and blue boxes for loss of DNA copy. Mutation allele frequency in the gene and the transcript (in parentheses) or DNA copy number are indicated under the corresponding gene name.

**Figure 2: Preclinical development of a novel GBM model in immunocompetent mice**. This model comprises surgical resection followed by radio/chemotherapy that recapitulates the current GBM patient standard of care (Stupp protocol) in mice. **A)** Schematic representation of the experimental design and comparison between human and the mouse model. **B)** Schematic representation of the mouse model with the 3 major steps including "Injection" of GL261 cells (orthotopic approach), 14 days later "Resection" of tumors using fluorescein labelling, and finally Stupp-like "Treatment". During resection, the skull was removed and the tumor contour was defined after injecting fluorescein and applying UV source on the tumor site. After aspiration of the tumor material, the resection cavity was filled with hemostatic materials before implanting a teflon prosthesis (replacing the removed bone) and the skin sewn. The Stupp treatment combined irradiation and chemotherapy (temozolomide/TMZ) – the surgical procedure is also reported in Movie S1.

**Figure 3: Development and analysis of the establishment of a Stupp-like protocol in mice. A)** At sacrifice, brains were collected, fixed in PFA, embedded in paraffin prior to be analyzed using immunohistochemistry using anti-vimentin antibodies (CTR: no injection; NS: no surgery; S: surgery only; SIT:surgery/irradiation/TMZ). **B)** Kaplan-Meier representation of mouse survival under this regiment (green: non-resected, blue: surgical resection, orange: surgical resection + radio/chemotherapy). **C-D)** Immunohistochemical analysis and quantitation of tumor angiogenesis post-resection. Abnormal vessels are indicated by arrows. **E-F)** Immunohistochemical analysis and quantitation of tumor infiltration/invasion post-resection. The migration distance of tumor cells from the tumor core in the non-resected and resected conditions is indicated by arrows.

**Figure 4: Evaluation of the impact of IRE1 inhibition by MKC8866 on GL261 cell response to stress. A)** Impact of MKC8866 treatment on IRE1 signaling as monitored using RT-qPCR analysis of XBP1 mRNA splicing upon time-course treatments with TUN (2 μg/ml) or TMZ (800 μM) (top). Expression of XBP1s protein following 8h of TUN or TMZ treatment in the presence or not of MKC8866 as detected using Western blotting (bottom). B) Impact of MKC8866 treatment on the expression of the XBP1s target gene ERdj4 as monitored using RT-qPCR. **C)** Impact of MKC8866 on TUN- and TMZ-induced ATF4 expression and the phosphorylation of eIF2α as monitored using Western blot. **D)** Impact of MKC8866 treatment on other arms of UPR signaling induced by TMZ as monitored using RT-qPCR analysis of HERPUD1, GRP94 (both reporting for ATF6 signaling) and CHOP (reporting for PERK signaling) mRNA expression. **E)** Impact of MKC8866 treatment on the sensitivity of GL261 cells to TMZ treatment in the presence or absence of radiation.

**Figure 5: Impact of IRE1 inhibition on tumor development under Stupp-like treatment**. **A)** Schematic representation of the experimental procedure and mouse survival. **B)** Macroscopic images of the brains following injection of GL261-Luc cells, surgical resection and treatment with ctrl plug (blue), MKC8866-containing fibrin microgels (grey); ctrl plug + Stupp (red) and MKC8866-containing fibrin microgels + Stupp (green). **C)** Quantification of tumor necrosis upon different treatments. **D)** Impact of IRE1 inhibition on tumor development under Stupp-like treatment - Kaplan-Meier representation. p value between Stupp and Stupp+MKC8866 (0.0146 – 10 μM (green) and 0.0118 – 100 μM (orange)).

**Figure 6: Immunohistochemical analysis of GL261-derived tumors following *in vivo* treatments**. **A**) Activated Caspase 3 (apoptosis) immunostaining sections from tumors collected at sacrifice. **B**) Ki67 (proliferation) immunostaining sections from tumors collected at sacrifice. **C**) IBA1 (macrophages and microglial cells) immunostaining sections from tumors collected at sacrifice. **D**) CD31 (endothelial cells) immunostaining sections from tumors collected at sacrifice. In each case at least 5 tumors per condition and at least 2 fields per tumor were analyzed. NS: non-significant.

**Figure 7: Analysis of GL261-derived cell lines following *in vivo* treatments**. **A**) Characterization of the derived lines regarding their sensitivity to MKC8866 (top) or TMZ (middle), and regarding their proliferation ability. Twelve lines were analyzed in multiple experiments (n > 4). Shown is the average ±SD. **B**) RNAseq analysis of the different derived cell lines and representation as heat map. Hierarchical clustering was performed as described in the methods section.

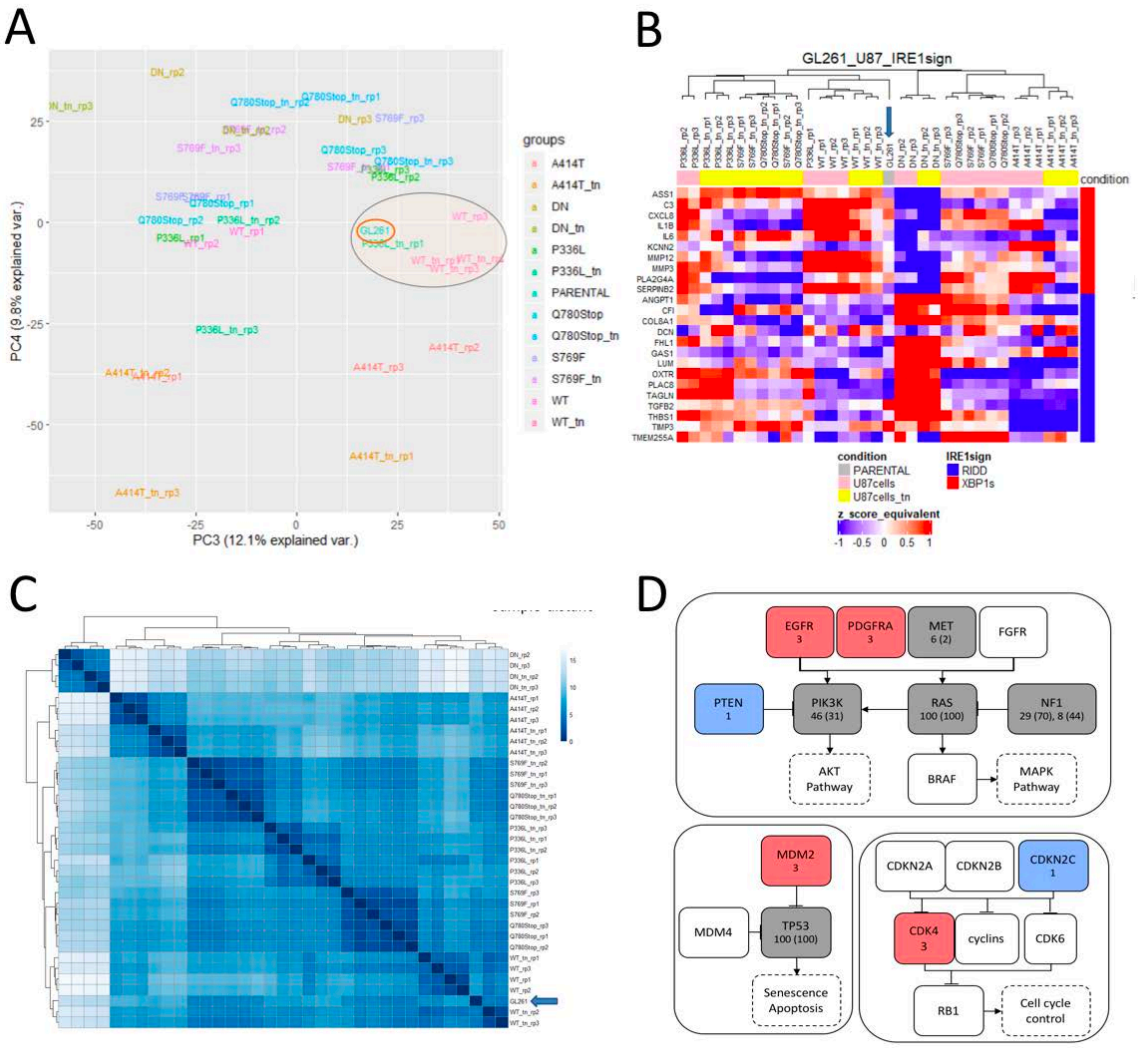


FIGURE 1

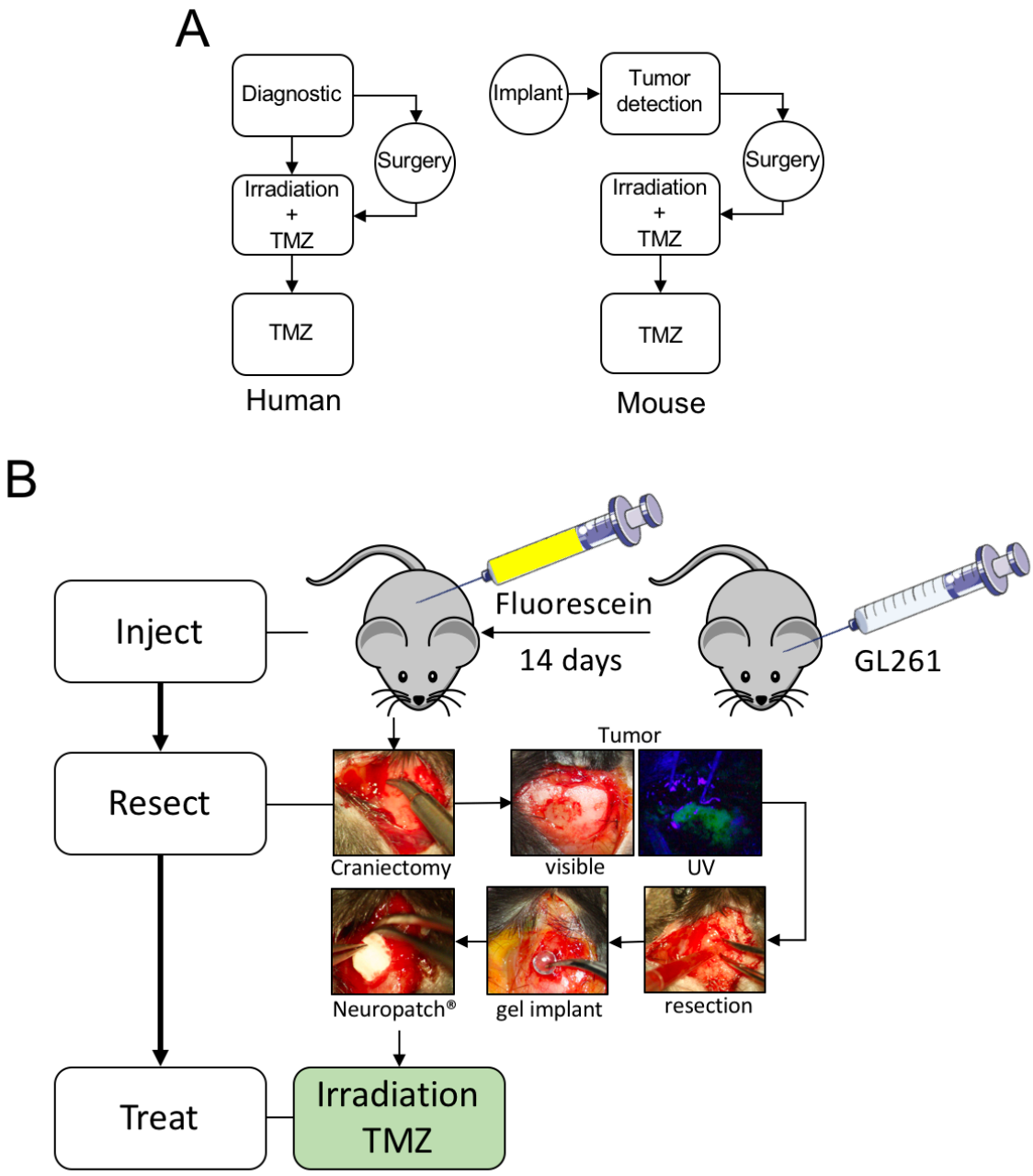
A
Diagnostic
Surgery
Irradiation + TMZ
TMZ
Human
Implant
Tumor detection
Surgery
Irradiation + TMZ
TMZ
Mouse
B
Inject
Fluorescein
14 days
GL261
Resect
Tumor
Craniectomy
visible
UV
Neuropatch®
gel implant
resection
Treat
Irradiation TMZ

FIGURE 2

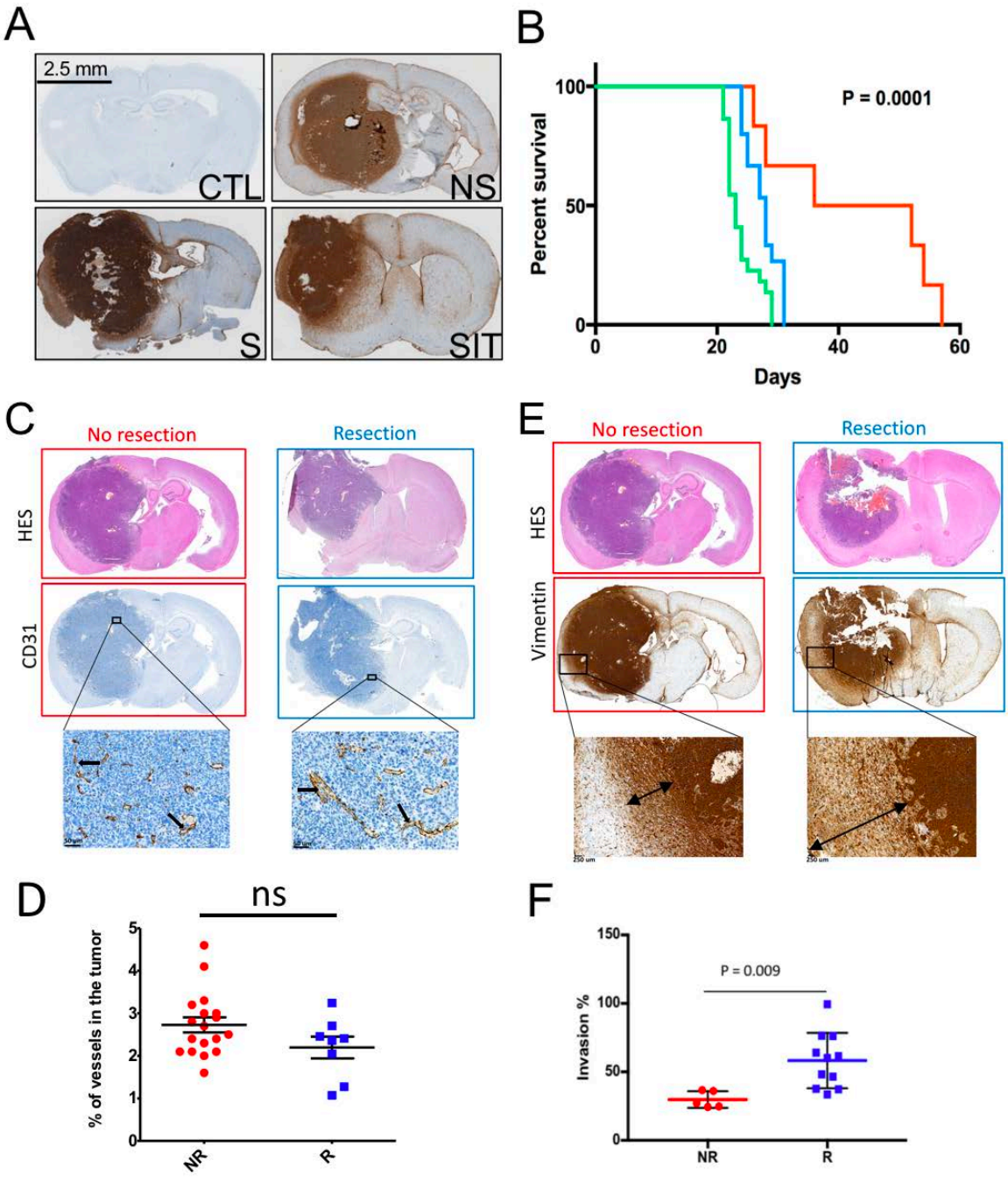
A
2.5 mm
CTL
NS
S
SIT
B
Percent survival
100
50
0
0
20
40
60
Days
P = 0.0001
C
No resection
Resection
HES
CD31
E
No resection
Resection
HES
Vimentin
D
ns
% of vessels in the tumor
5
4
3
2
1
0
NR
R
F
Invasion %
150
100
50
0
P = 0.009
NR
R

FIGURE 3

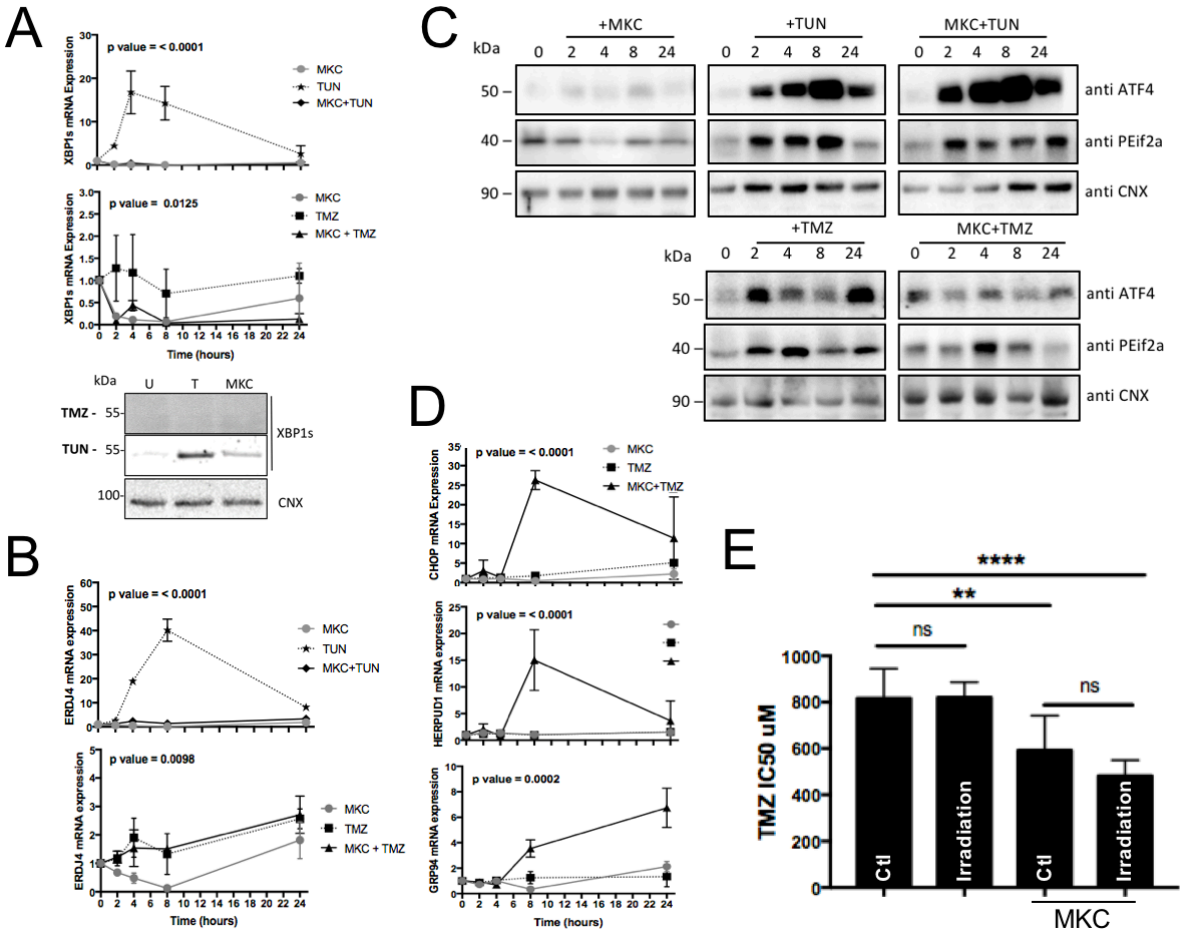


FIGURE 4

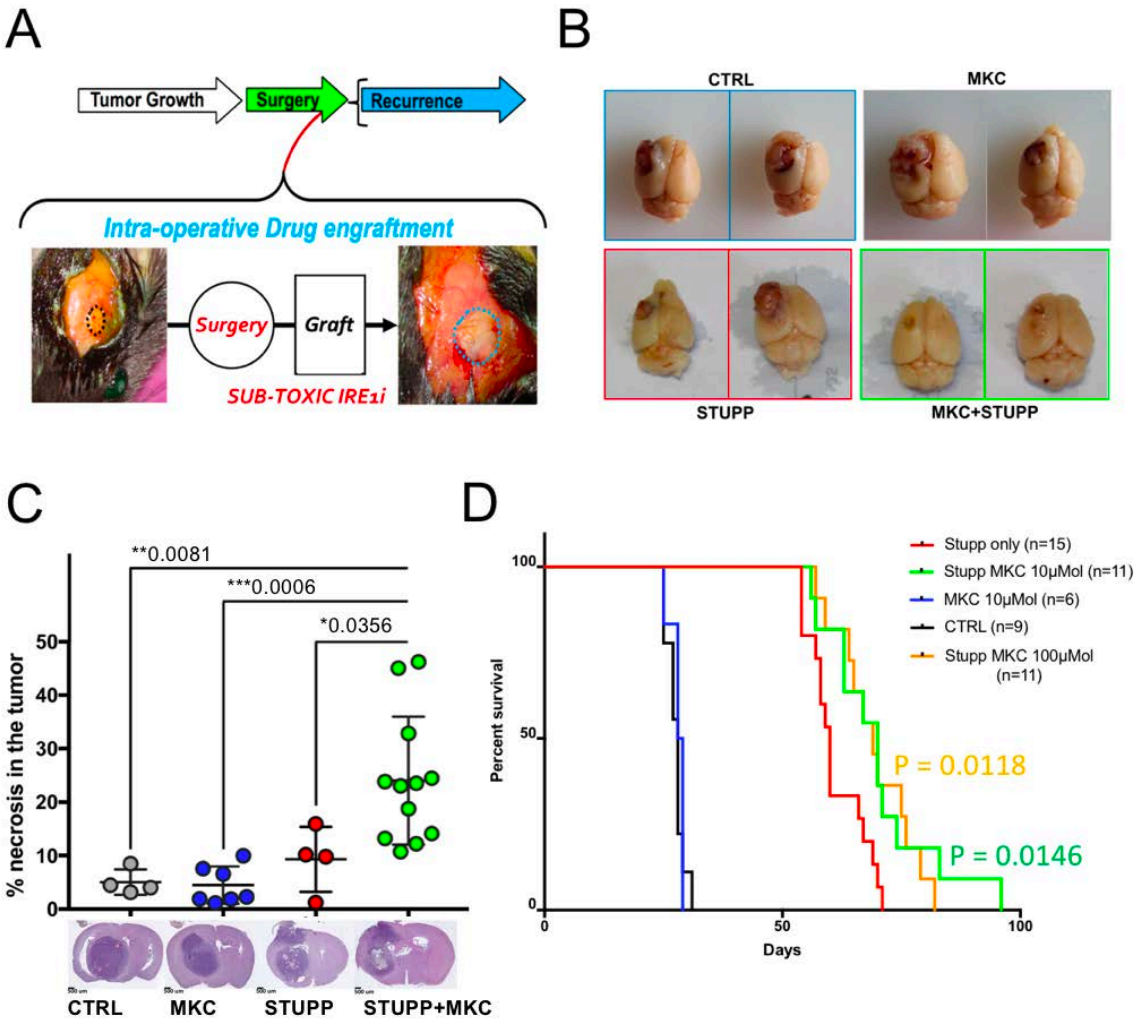


FIGURE 5

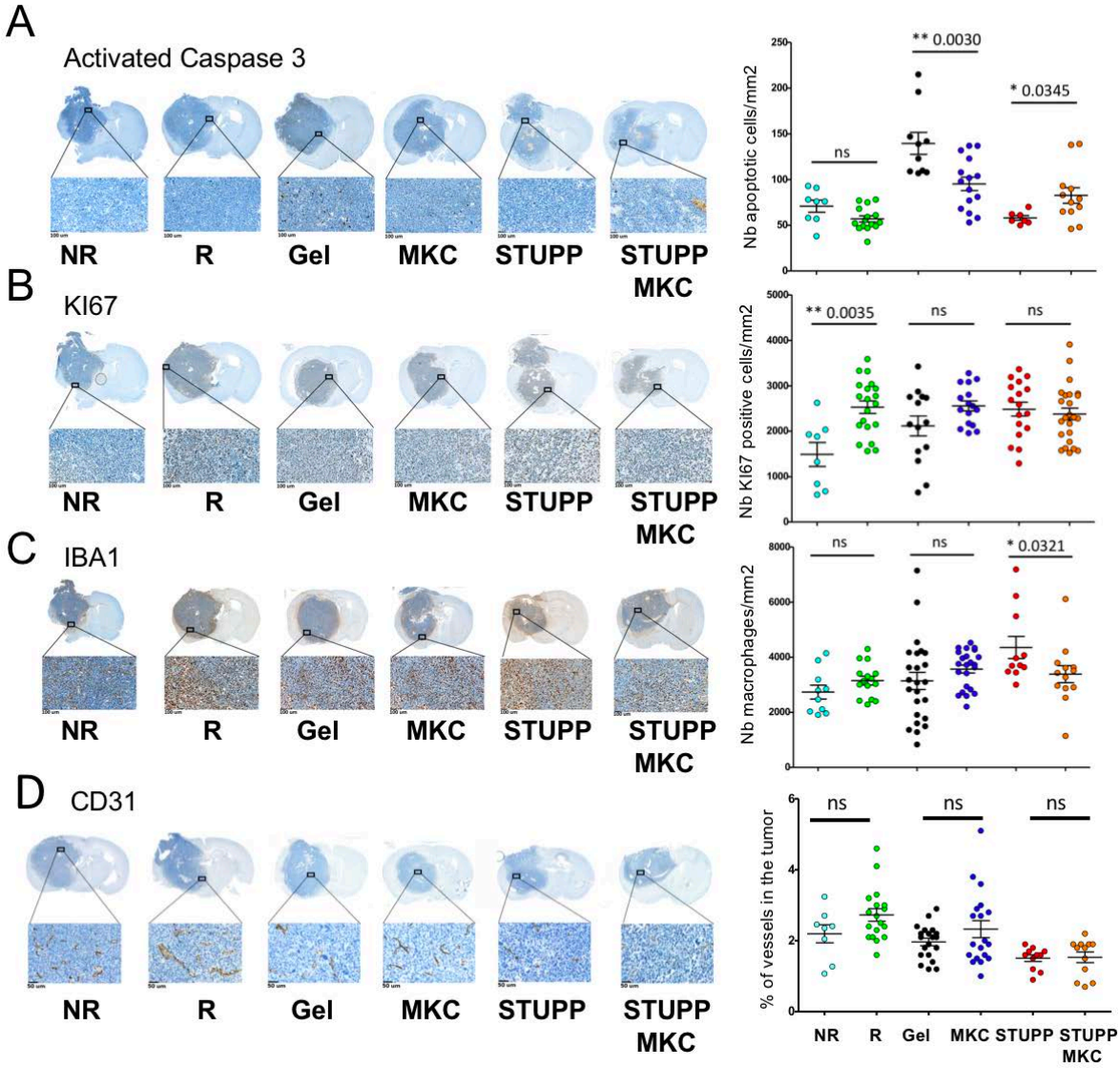


FIGURE 6

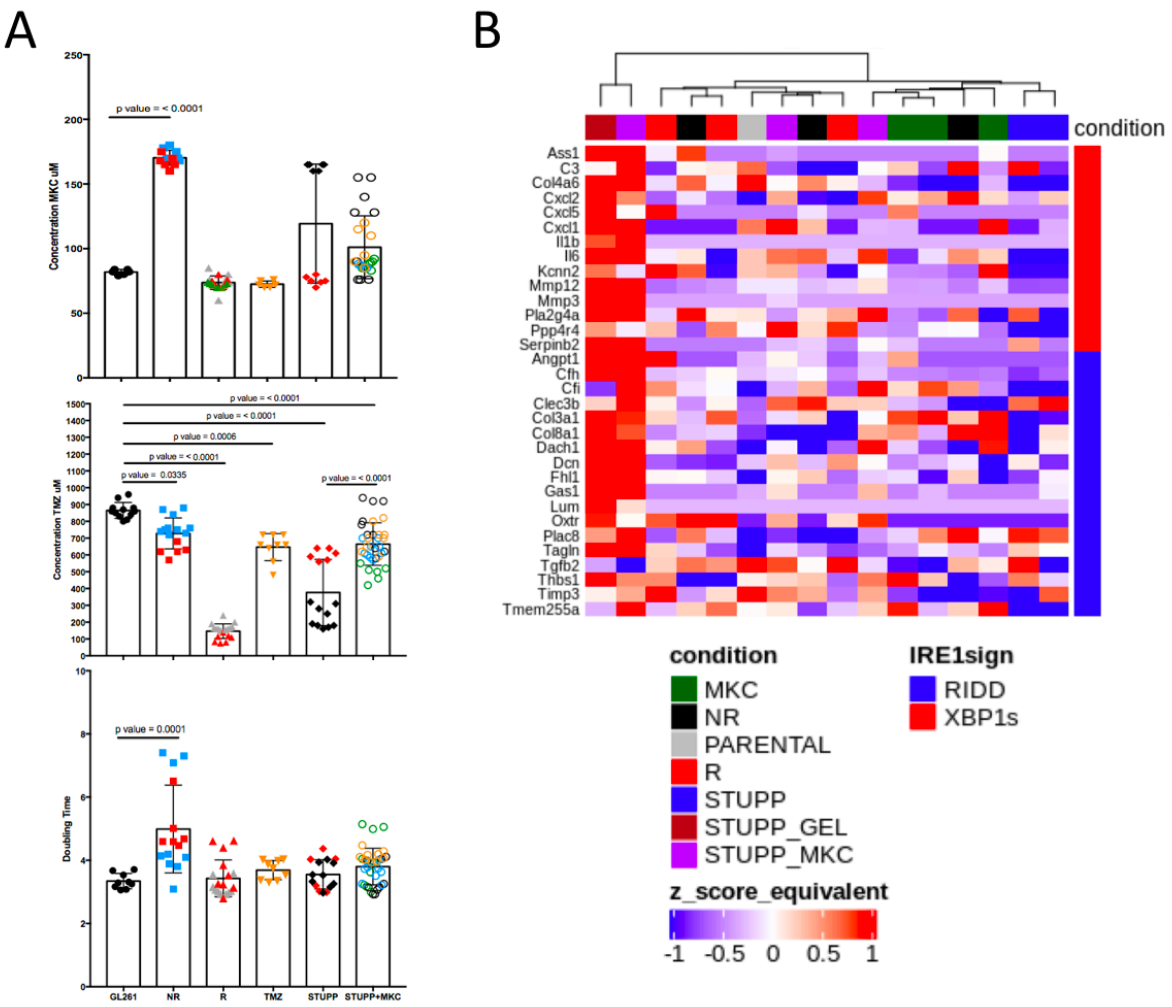


FIGURE 7